Available online at www.sciencedirect.com
ScienceDirect
Advances in Space Research 43 (2009) 1732–1739
ADVANCES IN SPACE RESEARCH (a COSPAR publication)
www.elsevier.com/locate/asr

Modeling medium-scale TEC structures, observed by Belgian GPS receivers network

I. Kutiev [a,b,*], P. Marinov [c], S. Fidanova [c], R. Warnant [d]

[a] Ebro Observatory, CSIC – Universitat Ramon Llull, 43520 Roquetes (Tarragona), Spain
[b] Geophysical Institute, Bulgarian Academy of Sciences, Acad. G. Bonchev, bl. 3, Sofia 1113, Bulgaria
[c] Institute for Parallel Processing, Bulgarian Academy of Sciences, Acad. G. Bonchev, bl. 25A, Sofia 1113, Bulgaria
[d] Royal Institute of Meteorology of Belgium, Avenue Circulaire 3, B-1180, Brussels, Belgium

Received 1 November 2007; received in revised form 3 July 2008; accepted 3 July 2008

Abstract

GALOCAD project "Development of a Galileo Local Component for the nowcasting and forecasting of atmospheric disturbances affecting the integrity of high precision Galileo applications" aims to perform a detailed study on ionospheric small- and medium-scale structures and to assess the influence of these structures on the reliability of Galileo precise positioning applications. GPS-derived TEC (total electron content) is obtained from the Belgium Dense Network (BDN), consisting of 67 permanent GPS stations. An empirical 3-D model is developed for studying these ionospheric structures. The model, named LLT model, described temporal variations of TEC in latitude/longitude frame (46°, 52°)N and (−1°, 11°)E. The spatial variations of TEC are modeled by Tchebishev base functions, while the temporal variations are described by a trigonometric basis. To fit the model to the data, the observed area is divided into bins with (1° × 1°) geographic scale and 6 min on time axis. LLT model is made flexible, with varying number of coefficients along each axis. This allows different degree of smoothing, which is the key element of the present approach. Model runs with higher number of coefficients, capturing in details medium-scale TEC structures are subtracted from results obtained with smaller number of coefficients; the latter represent the background ionosphere. The residual structures are localized and followed as they travel across the observed area. In this way, the size, velocity, and direction of the irregular structures are obtained.

Keywords: MSTIDs; GPS positioning; TEC modeling; Ionospheric disturbances

1. Introduction

The ionospheric irregularity structures are known to propagate away from their areas of origin, driven by atmospheric gravity waves. The moving ionospheric structures are known also as Travelling Ionospheric Disturbances (TIDs). In respect to their spectral parameters, TIDs are divided into three main groups: large-scale TIDs with a wavelength more than 500 km and period of 0.5–3.0 h and middle-scale TIDs (MSTIDs) with a wavelength of 50–500 km and periods 0.2–1.0 h. The other group represents the smallest scale size TIDs (SSTIDs) with a wavelength less than 50 km and period of several minutes.

MSTIDs have horizontal phase speed of 100–300 m/s and occur more frequently than LSTIDs. Their generation is not well understood, although many possible mechanisms have been proposed, such as orographic effects (Beer, 1974), wind shear (Mastrantonio et al., 1980), solar terminator (Beer, 1978; Somiskov, 1995), tropospheric effects (Bertin et al., 1978), breaking of atmospheric tides (Kelder and Spoelstra, 1987), etc. All these mechanisms do not include geomagnetic activity as a primary driver, although some non-linear interactions with LSTIDs are also assumed (Beach et al., 1997).

MSTIDs have been measured by various techniques, such as ionosondes (Bowman, 1990), HF Doppler (Waldock and

* Corresponding author. Address: Geophysical Institute, Bulgarian Academy of Sciences, Acad. G. Bonchev, bl. 3, Sofia 1113, Bulgaria.
E-mail address: ivankutiev@yahoo.com (I. Kutiev).

0273-1177/$36.00 © 2008 COSPAR. Published by Elsevier Ltd. All rights reserved.
doi:10.1016/j.asr.2008.07.021

Jones, 1987), satellite beacon (Evans et al., 1983), ground radar (Ogawa et al., 1994) and airglow imaging (Shiokawa et al., 2003). Comprehensive reviews on atmospheric gravity waves and mesoscale ionospheric disturbances are given by Hunsucker (1982), Whitehead (1989) and Mathews (1998). GPS-derived TEC, in particular, has proven to be most useful in studying those disturbances, which affect the GPS positioning accuracy. There are two main approaches to MSTID studies: single station time series analysis and image recognition analysis. First approach is well developed by Warnant (1998), Warnant et al. (2000, 2007) and Hernandez-Pajares et al. (2005, 2006). Second approach, used by Kodake et al. (2006) and Otsuka and Amaraki (2006), is based on the data inferred from the dense Japanese GPS network, containing more that 1000 dual-frequency receivers within Japan territory. These authors identified MSTIDs visually on the instant TEC maps and extracted their size and propagation parameters by tracing the structures as the time develops.

The present paper describes a new approach for studying MSTIDs, developed in framework of the project GALOCAD: "Development of a Galileo Local Component for the nowcasting and forecasting of atmospheric disturbances affecting the integrity of high precision Galileo applications". This project aims to perform a detailed study on ionospheric small- and medium-scale structures and to assess the influence of these structures on the reliability of Galileo precise positioning applications. GPS-derived TEC (total electron content) is obtained from the Belgium Dense Network (BDN), consisting of 67 permanent GPS stations. Here, TEC data, obtained from all GPS satellites in view during a certain time window is approximated by 3-D polynomial along latitude, longitude and time axes. Depending on the order, polynomial can capture disturbances with different size: low-order polynomials smooth out ionospheric disturbances, while higher order polinomials can capture localized TEC structures. The present approach subtracts low- from higher-order approximations to localize disturbance structures and follow their movement across the area. This paper describes the general approach, theoretical backgrounds and shows samples of model performance and dynamics of some localized TEC structures.

2. Data

Although GPS satellites can be viewed in a larger area, we constrain our analysis to the area (46°, 52°)N latitude and (−1°, 11°)E longitude. Fig. 1 presents TEC data gathered between 15:00 and 15:06 UT on day 359 (December 24) of year 2004. The color scale is shown on the right. The magnitude of data points is color coded, with 256 levels of spectra from violet to red. Five spots of data are seen, each representing BDN, seen from each of the five satellites in view. Note that two of the spots in the center of the mapping area are partially overlapped and show different TEC values. It is obvious that at any

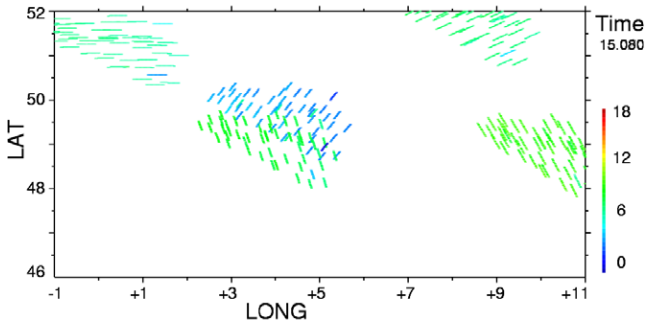

Fig. 1. Data inferred from GPS satellites in view between 15:00 and 15:06 UT on day 359 (Dec, 24) of 2004. Magnitude of data points is color coded, with 256 levels of spectra from blue to red. Visual inspection of the lat/long plots is an essential part of the analysis. TEC in units 10^{16} cm. (For interpretation of the references in colour in this figure legend, the reader is referred to the web version of this article.)

instant, a substantial part of the area does not contain data. To make a reliable fitting, we have to divide the area into proper number of sub-areas and accumulate data in them over certain time periods. We varied the size of sub-areas and time width in numerous combinations in order to optimize the size of the 3-D (latitude, longitude, and time) bins. The smaller is the bin size, the smaller is the size of disturbances that can be localized. The optimization procedure was interplay between two requirements: smaller bin size and the availability of data in the bins. We found that best combination is to use bins with size $1° \times 1°$ geographic scale and 6 min on time scale. This time scale is convenient for studying the middle-scale disturbances, because it is enough shorter than characteristic period (around 20 min) of the MSTIDs. The number 6 allows also presenting the time width as decimal part of the hour. To make a proper fitting of the data with analytical functions, we need to have data in all bins. In our case, the number of filled bins for every 6-min period is approximately 18% of total number of bins in the area. As will be show below, empty bins will be filled by a special algorithm by neighboring non-empty bins.

3. LLT model

As mentioned in Introduction, the present approach of studying MSTIDs requires approximation of acquired TEC data from BDN by analytical functions along the latitude, longitude and time. For convenience, we denote the approximation algorithm Latitude, Longitude, Time (LLT) model, although it is not yet a full-featured model. TEC data acquired from the area are approximated by a 3-D function, as the latitude and longitude variations are approximated by polynomials (Tchebishev's base functions), while for the time variations are used trigonometric functions (trigonometric base functions). This approach has been used in a number of empirical models (Marinov et al., 2004a,b; Kutiev et al., 2006; Kutiev and Marinov, 2007) and proved to represent accurately the observed data. The error assessment of the LLT model will be given below.

We use an analytic representation of the data by a function of three variables (LAT, LONG, TIME) = ($x1$, $x2$, t); $x1$ in the range [46, 52], $x2$ in the range $[-1, 11]$ and t in the range [0, 24]. We denote the number of coefficients related to the variables $x1$, $x2$, and t as $N1$, $N2$ and $N3$, respectively. The analytic representation of the data is a polynomial of the type:

$$F(x1,x2,x3;C) = \times \sum_{i1=1}^{N1}\sum_{i2=1}^{N2}\sum_{i3=1}^{N3} c(i1,i2,i3)B1(i1,x1)B2(i2,x2)B3(i3,t)$$

The data along variables $x1$ and $x2$ are approximated by Tchebishev base functions and the time variations are approximated by trigonometric basis. We denote with T the time range in which data are approximated. For the time range $T = 24$ h, we use a trigonometric basis containing sine and cosine functions, while for shorter time ranges ($T < 24$ h) we use cosine functions only. The reason for this is the fact that the time range $T = 24$ h contains diurnal variations of TEC and the pair of sine and cosine functions better approximate the data, while for the shorter time ranges cosine approximation is enough accurate. Approximation in different time ranges is explained in details later in the paper. We make substitutions in order to fit variables $x1$ and $x2$ in the interval $[-1, 1]$ and $x3$ in interval $[0, 2\pi]$ for $T = 24$ h, and $[0, \pi]$ for $T < 24$ h:

$$u1 = -1 + \frac{x1-46}{52-46}2 = -1 + \frac{x1-46}{3}$$

$$u2 = -1 + \frac{x2+1}{12}2 = -1 + \frac{x2+1}{6}$$

$$u3 = \frac{(t-T_0)}{T}2\pi \quad \text{for } T = 24\,h \quad \text{and}$$

$$u3 = \frac{(t-T_0)}{T}\pi \quad \text{for } T < 24\,h$$

Time variations are approximated by trigonometric basis:

$\{B3(i3,t)\} = \{1, \sin(u3), \cos(u3), \sin(2.u3), \cos(2.u3)\}$, ...

for the $T = 24$ h model and

$\{B3(i3,t)\} = \{1, \cos(u3), \cos(2.u3)\}$, ...

for the shorter model, $T < 24$ h.

The variables $x1$ and $x2$ are approximated by Tchebishev's base functions: $\{B1(i1,x1)\} = \{T_0(u1) = 1, T_1(u1) = u1, \ldots s, T_k(u1) = 2.u1T_{k-1}(u1) - T_{k-2}(u1), \ldots\}$, i.e $T_k(u1) = \cos(k.\arccos(u1))B2(i2,x2)$ is obtained similarly to $B1$ by replacing i1, $x1$ and $u1$ with i2, $x2$, $u2$, respectively. $C = \{c(i1,i2,i3)|i1 = 1, \ldots N1;\ i2 = 1, \ldots N2;\ i3 = 1, \ldots N3\}$. Solutions of the LSQ approximation is by minimizing:

$$\sum_{k=1}^{N}(f(k) - F(x1(k),x2(k),t(k);C))^2,$$

where $\{x1(k),x2(k),t(k),f(k)\}_{k=1}^{N}$ are data which we approximate. In domains with large gradients of the data, a Gibbs effect takes place (i.e. close to the area of the jump of the data the approximation achieves values greater than the maximal measured data and less than minimal one). To avoid this unacceptable effect, instead of approximating the function $f(k)$, we approximate the function $g(k) = \lg(f(k))$. In this case the approximated function is $G(k)$ and $F(k) = 10^{G(k)}$.

3.1. Filling the empty bins

To constrain the approximation in acceptable limits, we assign values to the empty bins by using the following procedure. We average first the measured TEC values in each non-empty bin. Every bin, except those at the boundaries, has 25 neighbor bins. We choose at first round the empty bins, which have at least 20 non-empty neighbors and assign to each of them values, being average of all neighbor's averages. Considering the newly filled bins non-empty, procedure repeats the filling until no empty bins exist with 20 non-empty neighbors. The second round we consider those empty bins having 19 non-empty bins and each next round procedure reduces the number of required non-empty bins by one. Practically, 5–6 rounds are enough to fill all empty gaps in the 24 h time range.

We found that it is better to use both individual data and bin averages in the fitting procedure, giving some preference to the average values in the bins. This preference depends on the time range T and the number of coefficients $N1$ and $N2$. We found that for $T = 24$ and the number of spatial coefficients 3–5, best result was obtained (lowest standard deviation of model from data) when a weight of 66 is assigned to the average values. So, the best combination is to fit the model over the measured data and weighted average in the bins.

4. Model performance

We show LLT model performance for TEC data acquired on day 359 (24 December) 2004. We varied the values of $N1$, $N2$ and $N3$ and assessed the performance of the model by the root mean square (RMS) deviation of model from the data. The model approximation with a defined set of coefficients is denoted as "model $(N1, N2, N3)$", for example, "model $(3, 3, 03)$" denotes a model approximation with $N1 = 3$, $N2 = 3$ and $N3 = 03$ (time coefficients can be greater than 10). Approximating the time variations, we use two different time ranges: the whole day ($T = 24$ h) and short range (T is less than 2 h). Both ranges have their own applications and will be described separately.

4.1. Approximations with time range $T = 24$ h

Fig. 2a is a model $(5, 5, 21)$ representation of the data shown in Fig. 1 in $1° \times 1°$ spatial grid size. Model presentation looks better when the model is shown in smaller grids, as it is in Fig. 2b. Here, grid size is $0.2° \times 0.3°$. Two structures are well localized: a maximum at 49°N

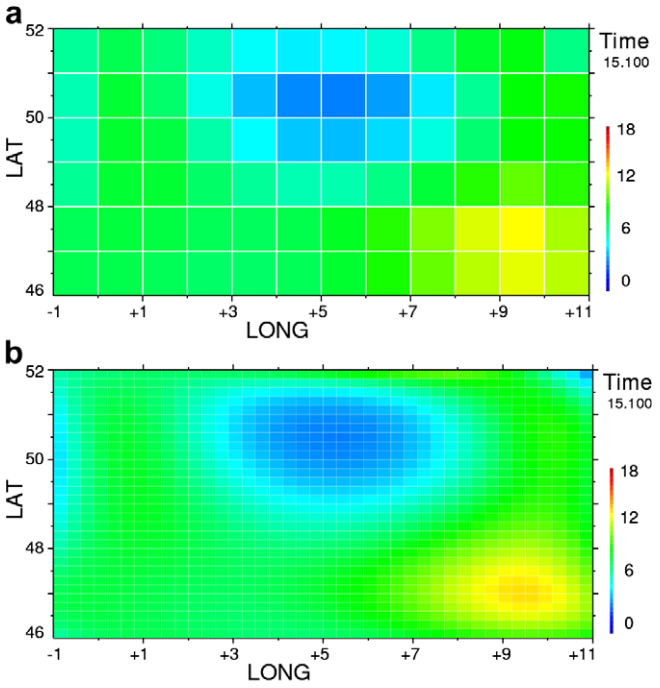

Fig. 2. (a) Model (5, 5, 21) representation of the data shown in Fig. 1, using bin size 1 × 1. (b) Model (5, 5, 21) representation of the data shown in Fig. 1, but using bin size 0.2 × 0.3.

and 9.5°E and a minimum at 50.5°N and 5°E. It is seen that the minimum is visible in the data from Fig. 1, while the maximum is found at a place where there are no data in this time interval. In this case, the model values are determined by the data from other time intervals.

It is expected that the approximation of time variations in T = 24 range is most important for the model performance. To give an idea how models with increasing $N3$ approaches the data, we show in Fig. 3a and b TEC data taken from the bin [49, 50]N and [3, 4]E as function on time. The upper panels show model approximation (red squares) and data (blue dots) during the whole day ($T = 24$ h). The left panel represents the model (5, 5, 11) and the right panel shows the model (5, 5, 21). The lower panels show respective deviations of model values from the data. Multiple curves represent the model every 0.2° inside the bin. Note, that the spread of model curves are not constant during the day, it depends on data configuration. This is an effect of small-scale structures in the data, not visible in the figure. The difference between the two approximations is well seen: the model (5, 5, 21) approximates better data variations.

4.2. Approximations with shorter time ranges T

As was pointed out above, approximations over the whole time range of 24 h require higher values of $N3$ and consequently, more computer resources. For MSTID studies in particular, the time range could be much smaller, but larger than 20 min (upper period limit). We run the model with two time ranges: $T = 48$ min and $T = 96$ min. To cover

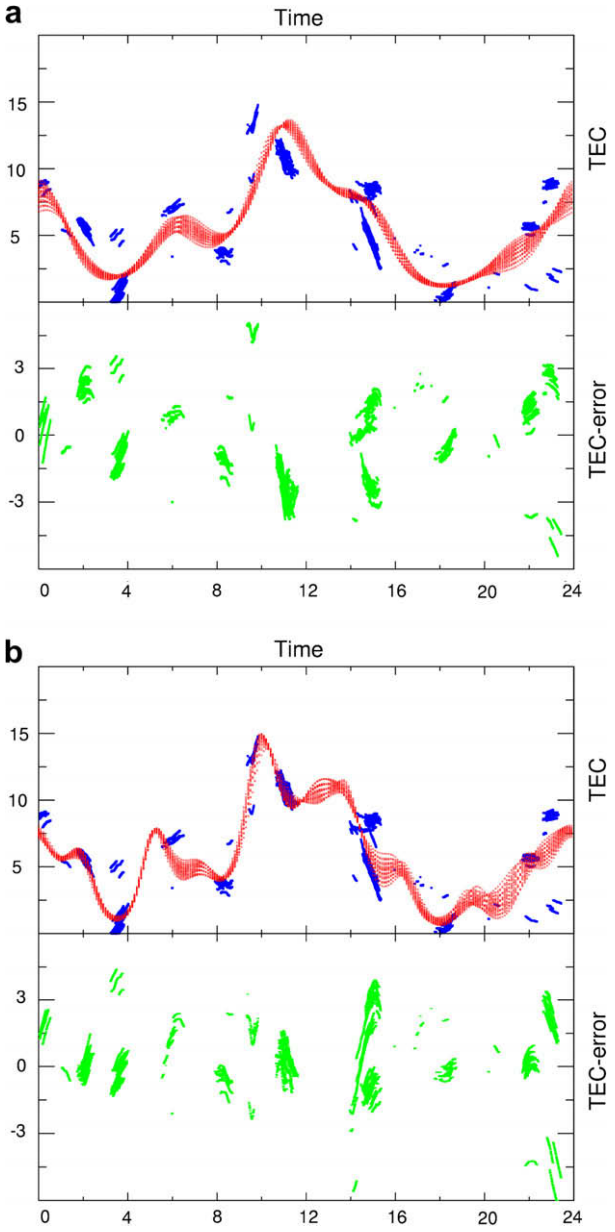

Fig. 3. (a) Top panel: TEC data acquired the bin [49, 50]N and [3, 4]E during the whole day 359 of 2004, is approximated by a model (5, 5, 11). Multiple curves are obtained by shifting lat and long by 0.2° inside the bin. Bottom panel: deviations of model from the data in TECU. (b) The same data as in Fig. 5a, but approximated by the model (5, 5, 21).

the whole day, the model was prepared to slide the time range starting from the beginning of the day, with a time shift of 6 min. The model value at any given moment is composed by the values of sequential short-range models, covering the given moment. For example, for models with $T = 96$ min, the model value at 10:02 h is composed by respective values from short-range models (08:30–10:02) (08:36–10:12),…(10:00–11:36), or totally from 16 models. The different values are weighted by a factor, reversely proportional to the time difference between their centers. Therefore, the model value at the moment 10:02 is an average of all weighted contributions. The same example, but

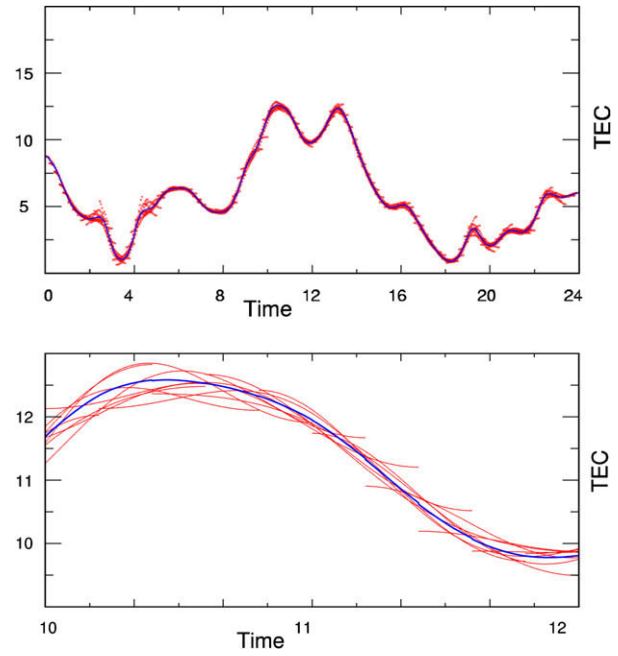

Fig. 4. Top panel: small dots represent individual model runs for approximation (3,3,03), with time range $T = 96$ min and time shift of 12 min. Blue curve is the weighted average from model runs in the range. Bottom panel: The model runs in top model are augmented in the time frame 10–12 UT. (For interpretation of the references in colour in this figure legend, the reader is referred to the web version of this article.)

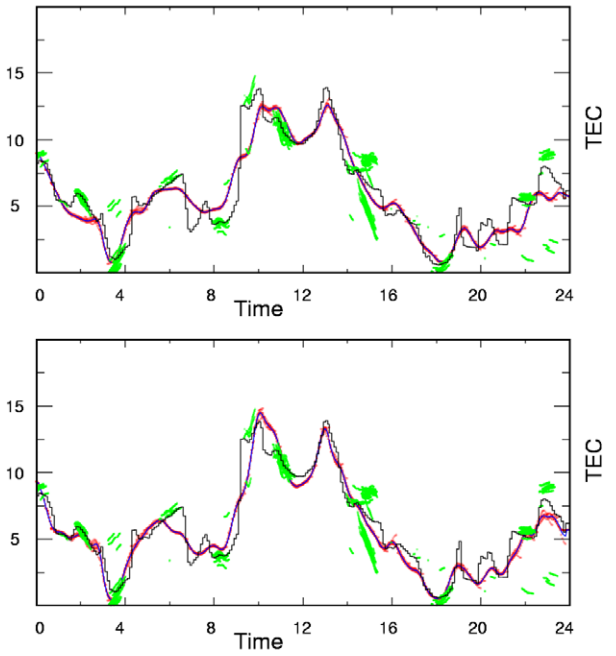

Fig. 5. Data (green dots), bin averaged (step-like curve), short-range model (red dots) and weighted model curve (blue curve) for the bin [49, 50]N and [3,4]E. (a) model approximation (3,3,05); (b) model approximation (5,5,05). (For interpretation of the references in colour in this figure legend, the reader is referred to the web version of this article.)

for the time range $T = 48$ min, the number of models, including the moment 10:02 are 8 (from 09:18 to 10:00).

Similar to Fig. 3, we represent in Fig. 4a the model approximation (3,3,03) with $T = 95$ min and time shift 12 min. The blue curve is the average of weighted individual model runs (red dots) and time shift 12 min. For better visualization, Fig. 4b augments the model curves of Fig. 4a within the period 10–12 UT. The individual short-range models, with several exceptions between 11:00 and 11:30, form a distinctive band around the main course of TEC variation. Note that the shorter T does not require high $N3$; here $N3 = 3$.

Increasing coefficients $N1$ and $N2$ also yields better approximations. Fig. 5 represents model curves (red lines) composed by short-range ($T = 96$ min) models (3,3,05) in the upper panel and (5,5,05) in the bottom panel, for the same bin [49, 50]N and [3,4]E, as above. For comparison, the green dots show the data and the step-like curve represents the average values (including the filled in) in the bins. Note, that the average models do not follow closely bin averages. It is clear that the model approximation (5,5,05) is closer to the data than approximation (3,3,05). We have found that the model performance is improved, when we increase $N1, N2$, along with $N3$, as they depend on each other.

5. Localizing TEC disturbances

The key element of the proposed approach is the use of the LLT model for localization of TEC disturbances. As was shown above, higher order polynomials (larger number of coefficients) capture more details of the irregular structure of TEC, than the lower order polynomials. We subtract a pair of short time range models with slightly different number of coefficients and suppose that the residuals represent local disturbances.

Fig. 6 shows the difference between short time range models ($T = 96$ min) in latitude/longitude frame for 16:30 UT. Upper plot shows the difference between models (3,3,3) and (5,5,3), and the lower plot shows the difference between models (5,5,5) and (5,5,3). Models with $N1 = N2 = 3$ approximate latitude and longitude with parabolas, which can make one extreme only. The structure shown on the upper panel has several extremes stretched from northwest to southeast. Obviously, this structure is produced by the difference of spatial approximations. Spatial approximation in this case modulates the magnitude of the structures, defined by the temporal approximation. Because the temporal approximation has trigonometric basis, $N = 3$ means two waves: the basic, with period of 96 min and its first harmonic, with period of 48 min. The lower panel represents the difference between models, having the same spatial approximation, but the spatial surface is described by a polynomial of 4th degree, capable of capturing three extremes. The structure is similar to that of the upper plot, but less expressed. Playing with higher order spatial polynomials, we found that the structures become less and less expressed. It is reasonable to assume that both, the spatial and temporal

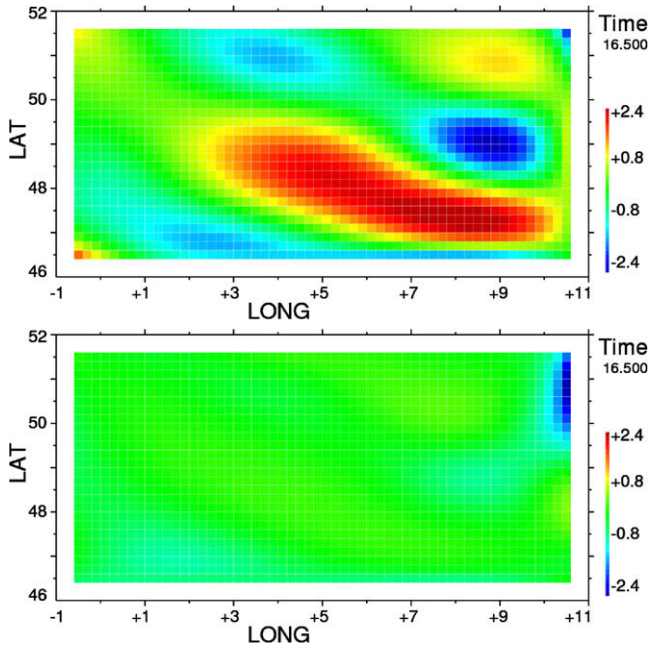

Fig. 6. Difference between short time range models ($T = 96$ min) at 16:30 UT. Top:(3, 3, 3)–(5, 5, 3); bottom: (5, 5, 3)–(5, 5, 5).

structures are coupled and characterized the size and duration of real disturbances.

Fig. 7 shows a sequence of 8 plots representing the difference between the models (3, 3, 3) and (5, 5, 3) from 16:18 to 17:00 UT, with a step of 6 min. The upper plot of Fig. 6 is one of sequential plots here. As was mentioned above, two maximums and two minimums are stretched in northwest-southeast direction. The sequence shows certain dynamics, mainly as a change in magnitude.

6. Discussion

For studying MSTIDs, we developed a model, based in a multivariable polynomial. The model approximates TEC data received from Belgian Dense Network (BDN) along latitude, longitude and time axes. The key elements of the model approach are the residuals obtained by subtraction of low order from higher order approximations. Higher order polynomials capture more detailed structures than those of lower order. Subtracting the two model values, we actually localize those disturbances, captured by higher order polynomial. This approach allows tracking the localized disturbances as they move across the area and thus estimate their direction and speed.

Important question is whether residuals represent the real disturbed structure of TEC. It could be possible that higher order polynomials form false extremes or large gradients at the borders. Our experience, gathered from numerous runs of the model, proves that this is not quite probable. From the general considerations, we conclude that the model can express extremes over the data only. In the areas without data, the bin averages form smoothed distribution and both, lower and higher order models would make the same fit. That is, their residuals would be with negligible magnitude. Because the averages weight 66 times more than individual data, the model can form an extreme if the number of data points in the bin considerably exceeds 66. Another indirect evidence of capturing real disturbances comes from the time development of localized structures. Fig. 7 shows that localized structures are sustainable and develop with time. Their behavior looks physically meaningful. The main conclusion that can be drawn is that localization is sustainable independently of the different approximations.

The size of localized structures is determined by residuals and does not represent the real size of disturbances, if we consider the latter as deviation from monthly median or average. We can consider the localized structures as top cuts of the existing disturbances, around their extremes. While the size is not significant parameter in the analysis, the change of magnitude, speed and direction are important for studying MSTIDs.

We studied extensively the RMS error as an estimate for assessing the model performance. RMS error, calculated over the whole day 359 of 2004, varies between 1 and 2 TEC units (TECU). In long models ($T = 24$), RMS error varies between 1.4 for $N3 = 25$ and 1.8 for $N3 = 13$. Increasing or decreasing $N1$ and $N2$ yields a reverse change of RMS error. For short models, RMS error is more sensitive to $N1$ and $N2$, than to $N3$. For models with $N1 = N2 = 3$, RMS error is around 1.5, and decreases to 1.2 for $N1 = N2 = 5$. It looks surprising that for the short models, RMS error is less sensitive to $N3$ than to $N1$ and $N2$. As was shown in Fig. 6, local disturbances are better expressed when subtract models with $N1 = N2 = 3$ than in the case with five coefficients. Indeed, for a fixed number of spatial coefficients, RMS error slightly decreases with increasing $N3$ and this decrease is stronger for lower order spatial approximation. This effect actually explains the fact, seen in Fig. 6, that model difference with $N1 = N2 = 3$ better localizes disturbances. The larger is the RMS error difference, the better disturbances are expressed. In this sense, subtracting models with different spatial coefficients localize better the disturbances.

7. Conclusions

We utilized a new approach for studying MSTIDs. TEC, derived by Belgium Dense GPS Network from an area $6° \times 12°$ geographic scale during specified time intervals, is approximated by 3-D polynomials of different order. The residuals, after subtracting approximations of lower order from higher order polynomials, are considered representative of local density disturbances. Corresponding software is named LLT (Latitude, Longitude, Time) model. In the present paper we provide theoretical formulations and samples of model performance. We believe that the present results give enough evidence of reliability of the

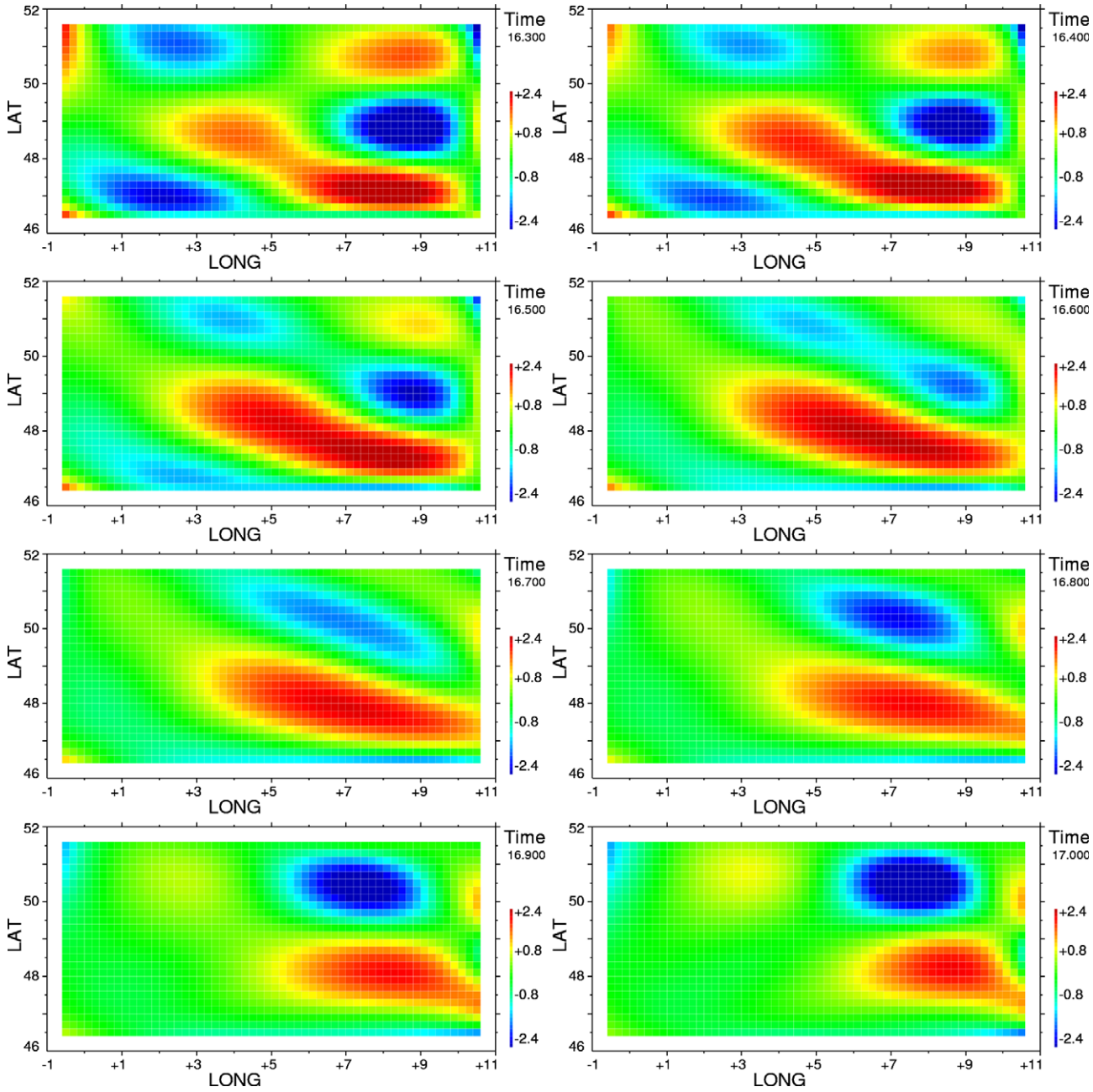

Fig. 7. Eight successive plots of difference between (3, 3, 3) and (5, 5, 3) models. The sequence starts at 16:18 UT from upper left column, with 6 min step, to the bottom right column. Time is marked at upper right of each plot.

proposed approach. Further work is planned for its verification and accuracy assessment.

Acknowledgement

This work is done in the framework of GALOCAD project (GJU/06/2423/CTR/GALOCAD).

References

Beach, T.L., Kelley, M.C., Kintner, P.M., Miller, C.A. Total electron content variations due to nonclassical traveling ionospheric disturbances: theory and global positioning system observations. J. Geophys. Res. 102 (4), 7279–7292, 1997.

Beer, T. Atmospheric Waves. Adam Hillger, London, 1974, 1974.

Beer, T. On atmospheric wave generation by the terminator. Planet. Space Sci. 26, 185–188, 1978.

Bertin, F., Testud, J., Kersley, L., Rees, P.R. The meteorological jet stream as a source of medium scale gravity waves in the thermosphere: an experimental study. J. Atm. Terr. Phys. 40, 1161–1183, 1978.

Bowman, G.G. A review of some recent work on midlatitude spread F occurrence as detected by ionosondes. J. Geomag. Geoelectr. 42, 109–138, 1990.

Evans, J.V., Holt, J.M., Wand, R.H. A differential-Doppler study of travelling ionospheric disturbances from Millstone Hill. Radio Sci. 18, 435–451, 1983.

Hernandez-Pajares, M., Juan, J.M., Sanz, J. Characterization of medium scale TIDs at mid-latitudes, Proceedings of Beacon Satellite Symposium 2004 (on CD-ROM), Trieste, October 2005.

Hernandez-Pajares, M., Juan, J.M., Sanz, J. Medium-scale traveling ionospheric disturbances affecting GPS measurements: spatial and temporal analysis. J. Geophys. Res. 111, A07811, doi:10.1029/2005JA011474, 2006.

Hunsucker, R.D. Atmospheric gravity waves generated in the high-latitude ionosphere: a review. Rev. Geophys. 20, 293–315, 1982.

Kelder, H., Spoelstra, T.A. Medium scale TIDs observed by radio interferometry and differential Doppler techniques. J. Atm. Terr. Phys. 49, 7–17, 1987.

Kodake, N., Otsuka, Y., Tsugawa, T., Ogawa, T., Saito, A. Climatological study of GPS total electron content variations caused by medium-scale travelling ionospheric disturbances. J. Geophys. Res. 111, A04306, doi:10.1029/2005JA011418, 2006.

Kutiev, I., Marinov, P., Watanabe, S. Model of topside ionosphere scale height based on topside sounder data. Adv. Space Res. 37 (5), 943–950, 2006.

Kutiev, I., Marinov, P. Topside sounder model of scale height and transition height characteristics of the ionosphere. Adv. Space Res. 39, 759–766, doi:10.1016/j.asr.2006.06.013, 2007.

Mastrantonio, G., Einaudi, F., Fua, D. Generation of gravity waves by jet streams in the atmosphere. J. Atmos. Sci. 33, 1730–1738, 1980.

Marinov, P., Oyama, K.-I., Kutiev, I., Watanabe, S. Low latitude model of Te at 600 km based on Hinotori satellite data. Adv. Space Res. 34, 2004–2009, 2004a.

Marinov, P., Kutiev, I., Watanabe, S. Empirical model of O^+–H^+ transition height based on topside sounder data. Adv. Space Res. 34, 2015–2022, 2004b.

Mathews, J.D. Sporadic E: current view and recent progress. J. Atm. Terr. Phys. 60, 413–422, 1998.

Ogawa, T., Ohtaka, K., Takashi, T., Yamamoto, Y., Yamamoto, M., Fukao, S. Medium- and large-scale TIDs simultaneously observed by NNSS satellites and MU radar, in: Kuo, F.S. (Ed.), Low-latitude ionospheric physics, COSPAR Colloq. Ser., vol. 7. Elsevier, Oxford, pp. 167–175, 1994.

Otsuka, Y., Amaraki, T. A statistical study of ionospheric irregularities observed with GPS network in Japan. Geoph. Monogr. Series 167, 181–271, 2006.

Shiokawa, K., Ihara, C., Otsuka, Y., Ogawa, T. Statistical study of nighttime medium-scale traveling ionospheric disturbances using midlatitude airglow images. J. Geophys. Res. 108 (A1), doi:10.1029/2002JA009491, 2003.

Somiskov, V.M. On mechanisms for the formation of atmospheric 489 irregularities in the solar terminator region. J. Atmos. Terr. Phys. 57 490 (1), 75–83, 1995.

Waldock, J.A., Jones, T.B. Source regions of medium scale travelling ionospheric disturbances observed at high latitudes. J. Atm. Terr. Phys. 49, 105–114, 1987.

Warnant, R. Detection of irregularities in the TEC using GPS measurements. Application to a mid-latitude station. Acta Geo. Geophy. Hung. 33 (1), 121–128, 1998.

Warnant, R., Kutiev, I., Marinov, P., Bavier, M., Lejeune, S. Ionospheric and geomagnetic conditions during periods of degraded GPS position accuracy: 2. RTK events during disturbed and quiet geomagnetic conditions. Adv. Space Res. 39, 881–888, 2007.

Whitehead, J.D. Recent work on mid-latitude and equatorial sporadic-E. J. Atm. Terr. Phys. 51, 401–410, 1989.